Electric Field Sensing Scheme Based on Matched $LiNbO_3$ Electro-Optic Retarders

Celso Gutiérrez-Martínez, *Member, IEEE*, and Joel Santos-Aguilar

***Abstract*—In this paper, a wideband-electric-field-sensing scheme that uses optically matched integrated optics electrooptic devices and coherence modulation of light is described. In a coherence modulation scheme, the integrated optics sensor detects the electric field and imprints it around an optical delay. The optical delay is generated by a birefringent optical waveguide in a lithium niobate ($LiNbO_3$) integrated optics two-wave interferometer. The modulated optical delay, acting as an information carrier, is transmitted through an optical fiber channel. At the receiver, light is demodulated by a second integrated optics two-wave interferometer, which also introduces a second optical delay. The optical delays on the sensor and demodulator are matched at the same value. The integrated optics demodulator measures the autocorrelation of light around the optical delay value, and the imprinted electric field is recuperated as a linear variation of the received optical power. The matching of the sensor and demodulator allows a direct detection of the electric field, giving a unique feature to this fiber-integrated optics scheme. The experimental setup described here uses two pigtailed $LiNbO_3$ electrooptic crystals: one acting as the electric field sensor and the other acting as the optical demodulator. The wideband sensing range on the experimental setup corresponds to frequencies between 0 and 20 kHz.**

***Index Terms*—Electric fields sensors, electrooptic modulators and demodulators, lithium niobate ($LiNbO_3$) integrated optics, optical coherence modulation, optical delays, wideband electric fields.**

I. Introduction

MEASUREMENT of high- and low-intensity electric fields, coming either from natural phenomena or from human activities, is an important subject because it impacts scientific, industrial, and commercial environments, among others. Static and dynamic electric fields are produced by different sources, including electric power equipment, power generation and distribution facilities, high-voltage transmission lines, telecommunication equipment, electromagnetic interferences, and human medical signals. More common electric field meters use conductive electrodes that are linked to the measuring electronics by cables, and very often, such arrangements distort the unknown field. Different techniques and apparatuses for the measurement of electric fields are reported in the technical literature, for instance, measurement of ac and dc electric fields in high-voltage transmission lines using fluorescent tubes and electromechanical field mills [1]–[4]. Human electroencephalograms are recorded by using sensitive electric field sensors in the form of probe electrode disks to characterize brain activity [5].

In the optical domain, a wide variety of electric-field-sensing schemes using electrooptic devices has been reported up to date. Most of such schemes use the Pockels effect, and integrated optics lithium niobate ($LiNbO_3$) Mach–Zehnder interferometers are used as electric field sensors. The sensed electric fields modulate the intensity of the light that passes through one arm of the Mach–Zehnder interferometer.

Sensor devices that either use electrodes or are electrodeless have been studied and integrated on different experimental sensing schemes. Using electrodes on the sensing devices give a high sensitivity, but the main disadvantage is that the electrodes may disturb the measured electric field. Such schemes are very well adapted to measure low-intensity electric fields (from millivolts to volts per meter), as found in telecommunication systems and electronic apparatuses [6]–[9]. Electrodeless sensors minimally disturb the measured field, but the sensitivity is relatively low, and such devices are better adapted to the measurement of high-intensity fields, ranging from some kilovolts per meter to hundreds of kilovolts per meter (4–2000 kV/m), as found in natural lightning strikes, high-power electrical facilities, and high-voltage transmission lines [1], [3], [10]–[12].

In an alternative approach, and instead of using Mach–Zehnder electrooptic devices, wideband electric field sensing using electrooptical retarders is described in this paper. In this case, the electric field modulates an optical delay, which is generated by a birefringent optical waveguide used as a two-wave interferometer. The modulation of optical delays is known as optical coherence modulation. Electric field detection using such a technique has been previously reported, describing the detection of 60-Hz electric fields [13]–[15]. In coherence modulation of light, electric fields are imprinted on light as a sequence of optical delays that are greater than the coherence time of the optical source. Coherence modulation of light uses electrooptic retarders, and practical realizations are based on $LiNbO_3$ electrooptic technology.

In a novel approach of implementing coherence modulation of light, in this paper, we describe the sensing of high-intensity and wideband electric fields, using electrodeless optically matched electrooptical retarders. In a previous paper, an experimental scheme was implemented using $LiNbO_3$ electrooptic sensors, and the demodulation process was ensured by an automated scanning Michelson interferometer [14]. In the improved sensing scheme described here, the system is fully implemented using fiber optic components and pigtailed electrodeless $LiNbO_3$ electrooptic retarders: one as the sensor

Manuscript received March 23, 2007; revised December 13, 2007.

The authors are with the Instituto Nacional de Astrofisica, Optica y Electrónica (INAOE), Puebla 72000, México (e-mail: cgutz@inaoep.mx).

Color versions of one or more of the figures in this paper are available online at http://ieeexplore.ieee.org.

Digital Object Identifier 10.1109/TIM.2008.917174

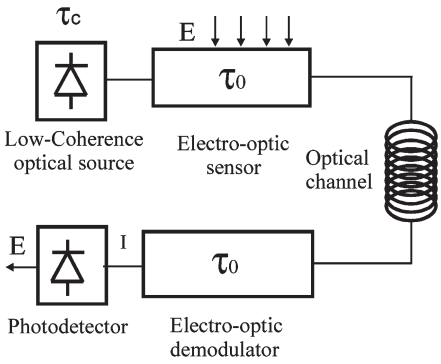

Fig. 1. Coherence-modulated electric field sensing.

and the other as the optical demodulator. In this case, the demodulation of the sensed electric field is directly realized by the integrated optics demodulator, which is designed to match the optical delay on the sensor. The wideband sensing scheme was successfully tested by detecting high-intensity electric fields, ranging from 20 to 350 kV/m, in a band between 0 and 20 kHz.

The proposed scheme can be useful for the detection and measurement of transient and steady-state electric fields, in a band up to 20 kHz, as can be found in natural and man-made environments.

In contrast to Mach–Zehnder interferometer sensors, a very attractive feature of coherence modulation is that it allows serial or parallel multiplexing of optical delays [16], and from this fact, multipoint sensing arrays can be proposed. Serial coherence multiplexing can be a promising technique in fiber optic schemes for distributed sensing arrays, as several optical delays can be cascaded over a single optical channel.

II. Theoretical Background

A. Operating Principle of the Proposed Sensing Scheme

To recall the operating principle, the block diagram of an integrated optics electric field sensor system, based on coherence modulation of light, is shown in Fig. 1. The system includes a low-coherence optical source, an electrooptic sensor (electrooptic retarder), an optical fiber channel, and a receiver module that is implemented by a second integrated optics retarder (coherence demodulator) and a wide-area slow photodetector. According to the block diagram, light coming from a low-coherence optical source is injected into the electrooptic sensor, which introduces an optical delay τ_0 that is greater than the source coherence time τ_c. In our practical setup, the optical delays are generated by $LiNbO_3$ electrooptic crystals, acting as two-wave interferometers. Such devices generate static optical delays (or, equivalently, optical path differences: OPDs), which can be modulated by an electric field. The electrooptic retarders that we used here are in-diffused optical waveguides in z-cut y-propagating $LiNbO_3$ birefringent slabs, which introduce OPDs as 45° polarized light is projected in orthogonal propagating TE and TM modes. Such modes travel in the optical waveguide at different velocities, as determined by the ordinary and extraordinary refractive index difference $(n_o - n_e) = 0.083$ at $\lambda_0 = 1318$ nm. A static OPD is then given as $d_0 = (n_o - n_e)L$, with L being the birefringent waveguide length. The operating principle is described in detail elsewhere [13].

On the sensing scheme, once the electric field is sensed, light is coherence modulated and transmitted through an optical fiber channel. At the receiver, light is demodulated using a second electrooptic retarder, which measures the autocorrelation of the received light around the sensor's OPD. This condition can be achieved by matching the optical delays of the electrooptic sensor and the optical demodulator, as shown in Fig. 2. As depicted in this figure, the electrooptic sensor introduces a static OPD d_0, and the demodulator also introduces the same OPD d_0. At the output of the optical demodulator, optical interference exists, and the measured optical intensity corresponds to the normalized autocorrelation of the transmitted light $g(d) = |g(d)| \cos((2\pi/\lambda_0)d)$. At an OPD d_0, the detected optical power is

$$P_r(d_0) = \frac{P_0}{4} + \frac{P_0}{8} g(0) \tag{1}$$

where $P_r(d)$ is the received optical power. P_0 is the average emitted power of the optical source, and λ_0 is the center optical wavelength.

To ensure a linear detection of the imprinted electric field, the receiver interferometer must be adjusted to a static OPD of $(d_0 \pm (\lambda_0/4))$. This adjustment is achieved either by using a quarter-wave optical plate or by designing the OPD $= (d_0 \pm (\lambda_0/4))$ on the demodulator.

When an electric field $E_z(t)$ is sensed by the coherence modulator, it induces a dynamic variation $\Delta d(t)$ on the OPD. On a z-cut $LiNbO_3$ birefringent crystal, the electric field is oriented on the z-axis of the crystal, taking advantage of the r_{13} and r_{33} linear electrooptic coefficients. The time-varying OPD is then given as

$$d(t) = d_0 + \Delta d(t) \tag{2}$$

where $\Delta d(t) = (\lambda_0/2)(E_z(t)/E_\pi)$, and E_π is the half-wave electric field given as

$$E_\pi = \lambda_0 / \left(r_{33} n_e^3 \Gamma_{\mathrm{TM}} - r_{13} n_o^3 \Gamma_{\mathrm{TE}}\right) L. \tag{3}$$

In (3), L is the electrooptic crystal length and represents the interaction length between the electric field and the optical wave, r_{13} and r_{33} are the electrooptic coefficients, Γ_{TE} and Γ_{TM} are the electric–optical overlapping coefficients. From (3), the half-wave electric field depends on the length of the electrooptic sensor. The longer the crystal is, the lower the half-wave electric field becomes, and hence, a higher sensitivity results, e.g., the longer sensors will allow the measurement of lower field intensities. In practical applications, the longest crystals are around 75 mm (3 in), which are limited by the $LiNbO_3$ commercial wafer sizes.

When the receiver is adjusted at the OPD d_0, according to (1), the detected optical power is given as

$$P_r(t) = \frac{P_0}{4} + \frac{P_0}{8} \cos\left(\pi \frac{E_z(t)}{E_\pi} - \frac{\pi}{2}\right) = \frac{P_0}{4} + \frac{P_0}{8} \sin\left(\pi \frac{E_z(t)}{E_\pi}\right).$$

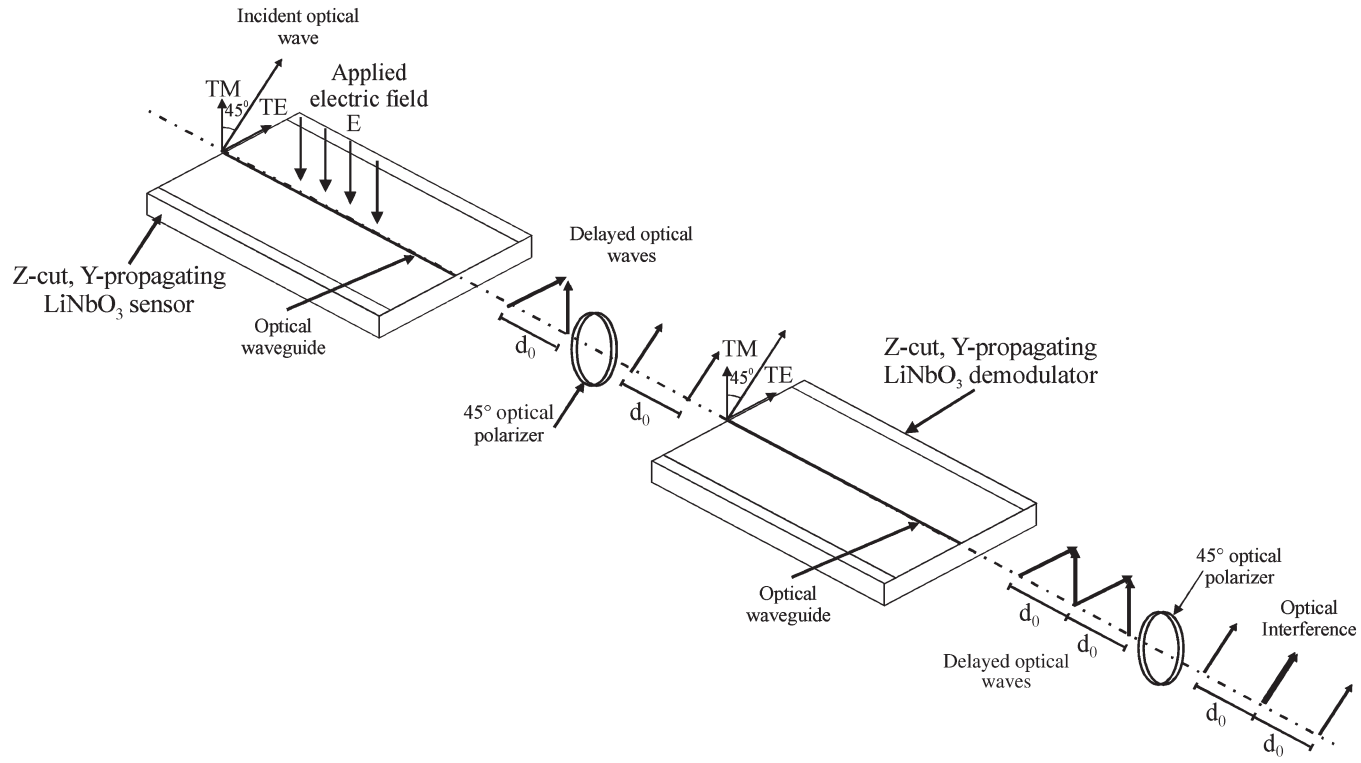

Fig. 2. Optical matching between the electrooptic sensor and the demodulator.

Additionally, if $E_z(t) \ll E_\pi$, in which $\sin(\pi(E_z(t)/E_\pi)) \approx \pi(E_z(t)/E_\pi)$, the measured optical power is then given as

$$Pr(t) = \frac{P_0}{4}\left(1 + \frac{\pi}{2}\frac{E_z(t)}{E_\pi}\right). \tag{4}$$

Equation (4) represents an intensity modulation, and the electric field is detected as a linear variation of the received optical power.

B. Frequency Response of the Sensing Scheme

The frequency response of the proposed electric-field-sensing scheme is determined by the modulation sensitivity of the $LiNbO_3$ sensing crystal, which is determined by its high relative permittivity $\varepsilon_r = \sqrt{\varepsilon_{13}\varepsilon_{33}} = 35$, where $\varepsilon_{13} = 44$, and $\varepsilon_{33} = 28$. As it has been very well established in theoretical and experimental work [17]–[21], its frequency response will depend on the nature of the interaction between the electric and optical fields. If the electric field is applied via lumped electrodes, by using parallel plates, the frequency response is a tradeoff of the optical–electrical interaction length L, which in this case is given by

$$f_m \cdot L = \frac{c}{\pi\sqrt{\frac{1+\sqrt{\varepsilon_{13}\varepsilon_{33}}}{2}}}. \tag{5}$$

Such a response is equivalent to around 2.2 GHz · cm.

C. SNR Performance

An important parameter for evaluating the system performance is the signal-to-noise ratio (SNR), which determines the minimum detectable electric field. The SNR is limited by the noise (spontaneous beat, thermal, and shot) at the photodetection process.

At the receiver, the instantaneous photodetected current is of the form

$$I(t) = RP_r(1 + m\,\cos\,\omega_m t) \tag{6}$$

where $R = (\eta q/h\nu)$ is the optical responsivity ($\eta = 0.7$ is the quantum efficiency, q is the charge unit, h is the Planck constant, and ν is the optical frequency), P_r is the received optical power, and m is the modulation index [the maximum index given by $m = (\pi E_{z0}/2E\pi)$]. From (6), the photodetected current can be expressed as

$$I = I_{\rm dc} + I_p(t)$$

where $I_{\rm dc} = RP_r$ is the average photocurrent, and $I_p(t)$ is the signal current with a mean square value $\langle I_p^2\rangle = (1/2)m^2R^2P_r^2$.

The SNR is then given as [22], [23]

$$\text{SNR} = \frac{\langle I_p^2\rangle}{\text{RIN}\,R^2P_r^2B + 2qI_{\rm dc}B + \frac{4kTB}{\rm R_e}}. \tag{7}$$

In this expression, RIN $R^2P_r^2B$ corresponds to the beat noise power, $2qI_{\rm dc}B$ is the shot noise power, and $4kTB/R_e$ is the thermal noise power. RIN is the relative intensity noise of the optical source, k is the Boltzmann constant, T is the absolute temperature, B is the electrical bandwidth, and R_e is the equivalent load resistance of the photodetector.

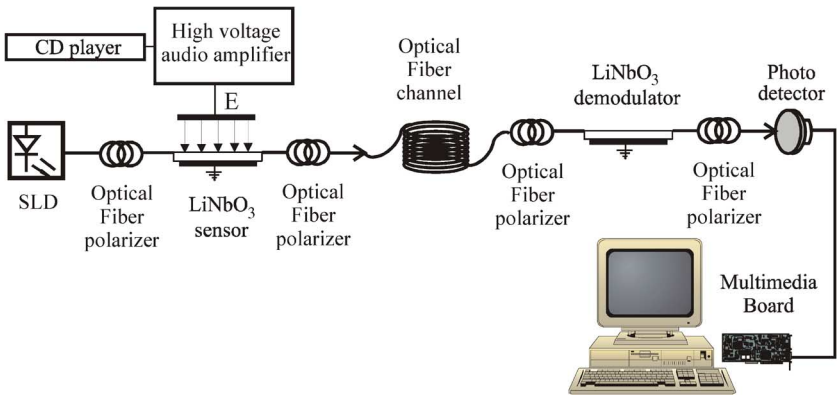

Fig. 3. All-fiber sensing experimental setup.

To evaluate the SNR, the three main types of noise are considered. The beat noise, which is related to RIN, comes from the incoherent optical source, whereas the shot and thermal noise are associated with the photodetection process [22]–[27].

In our experimental setup, the noise sources are related to the characteristics of the optical source, the photodetector, and the associated electronic amplifier. In our scheme, the optical source is a broadband superluminiscent semiconductor diode (SLD), emitting in a Gaussian spectrum around a center wavelength of $\lambda_0 = 1318$ nm, and showing a spectral width of around $\Delta\lambda = 60$ nm. The received average optical power is about 0.5 μW, and the electrical bandwidth on the photoreceiver is 20 kHz. After the theoretical basis, as explained in [22] and [26], such a Gaussian optical source will exhibit a maximum RIN $= (0.66/\Delta\nu)$, with $\Delta\nu = c\Delta\lambda/\lambda_0^2$ being the optical bandwidth. In such a case, the RIN is about -132 dB/Hz. This corresponds to a spontaneous beat noise power of about -188 dBm. A similar calculation regarding the shot noise power gives -176 dBm.

Suppose that our system is only shot noise limited. By using (3), (4), and (6), the SNR is [11], [24]

$$\text{SNR} = \frac{\eta m^2 P_r}{2h\nu B}.$$

The minimum detectable external electric field is obtained when SNR $= 1$. Under such a condition, using (3) and the modulation index m, we have

$$E_{z\,\min} = \varepsilon_r \frac{4}{\pi}\sqrt{\frac{2h\nu B}{\eta P_r}}E_\pi \quad \text{(in volts per meter)}. \tag{8}$$

To illustrate the minimum detected values, let us consider a $LiNbO_3$ sensor crystal with a length of 13 mm and permittivity $\varepsilon_r = 35$. The minimum detected electric field, in agreement to (8), is about 2 kV/m. For comparison, when using a crystal of 35 mm and the same optical parameters, the minimum detected field is about 0.7 kV/m. This theoretical calculation shows that the sensitivity of electrodeless sensors depends on the crystal dimensions and on the optical parameters.

III. Experimental Setup

The experimental wideband-electric-field-sensing scheme is shown in Fig. 3. The system is implemented by a wide-spectrum SLD, emitting at a center wavelength $\lambda_0 = 1318$ nm, an optical bandwidth of about $\Delta\lambda = 60$ nm, an average emitted power of 500 μW, and a coherence length of about 60 μm.

The electric field sensor is a fiber pigtailed z-cut y-propagating $LiNbO_3$ integrated optics coherence modulator, which introduces a static OPD d_0. The optical demodulator is also a pigtailed electrooptic birefringent slab, which introduces the same OPD d_0. The 45° optical fiber polarizers ensure the propagation of TE and TM optical modes on the electrooptic birefringent waveguides.

A 500-m optical fiber channel completes the experimental setup.

To implement the electric-field-sensing system, the static OPDs of the coherence sensor and the optical demodulator were first measured. Two almost identical 13-mm-long optical birefringent slabs were used. The 13-mm-long slabs will introduce a theoretical OPD $d_0 = (n_o - n_e)L$ of 1.079 mm at $\lambda_0 = 1318$ nm. To demonstrate the matched condition of the OPDs, the sensor and demodulator are cascaded, and the transmitted light is measured by a scanning Michelson interferometer. To ensure a linear detection of the optical signal, the demodulator crystal was designed to introduce an OPD $d_0 \pm (\lambda_0/4)$; however, $\lambda_0/4 = 325$ nm is so short that it is very difficult to resolve when constructing and polishing the crystal optical faces. A finer matching of the OPD on the demodulator can be achieved by providing dc electrodes, and a control voltage can be used to shift the OPD by $\lambda_0/4$. After constructing the electrooptic sensors, Fig. 4(a) shows the measured matched OPDs. As can be observed, the electrooptic sensors exhibit static OPDs near $d_0 = 1$ mm, and a zoom of the interference fringes around 1.08 mm is depicted. This fine measurement confirms that interference exists only in the range of the coherence length of the optical source, as the fringe patterns are slightly spatially shifted, thus ensuring the demodulation of the sensed electric field. This represents a particular feature of this sensing scheme.

The measured electric field can be displayed on a standard oscilloscope or calibrated in full scale to be digitized and stored in a personal computer for further signal processing.

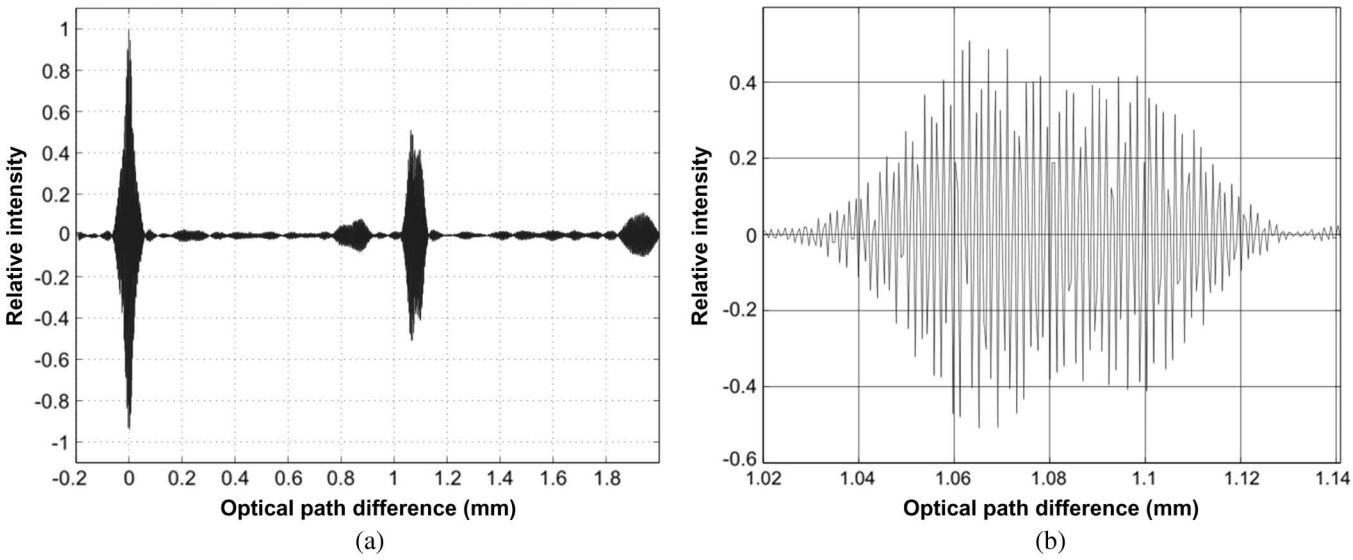

Fig. 4. (a) Matched OPDs. (b) Zoom at the interference pattern.

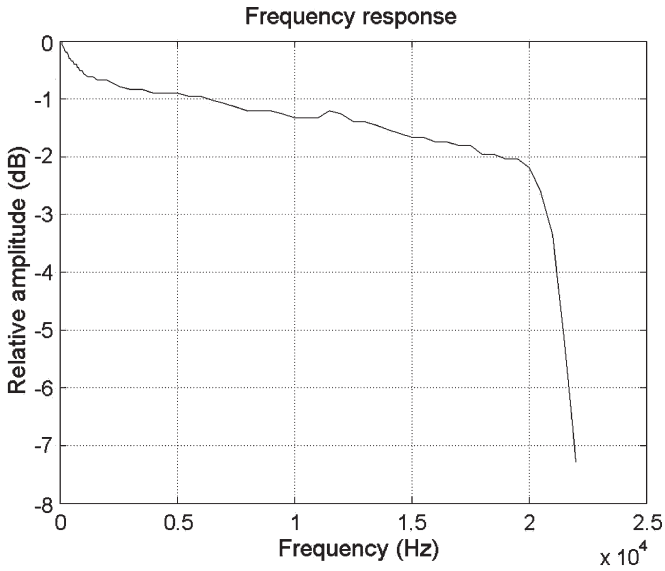

Fig. 5. Frequency response of the electric field sensing setup.

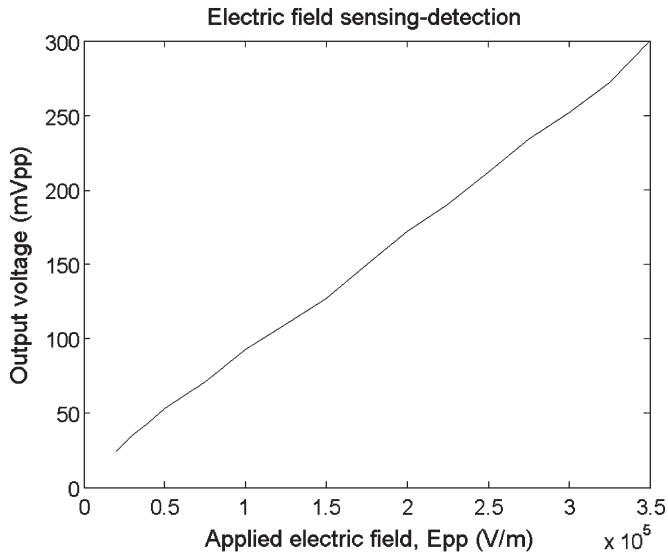

Fig. 6. Electric field sensing–detection range.

IV. Experimental Results and Discussion

To test the complete fiber-integrated optics sensing scheme, an initial experiment consisted of applying sinusoidal electric fields to the coherence electrooptic sensor in a frequency band of up to 20 kHz. The modulated light was then transmitted through the 500-m optical fiber channel. At the receiver, light was measured by the electrooptic coherence demodulator, which was already matched at a static OPD of 1.08 mm. The maximum frequency response of the sensing scheme was limited to 20 kHz by the high-voltage driving amplifier and by the photoreceiver, which is integrated by a wide-area p-i-n photodetector and a narrowband electronic amplifier. The frequency response of the experimental scheme, between 0 and 20 kHz, is depicted in Fig. 5. The electric field was generated by a signal generator and then amplified to a high voltage, which was applied to two parallel plates that were not in contact with the electrooptic sensor. AC electric fields that ranged from 10 to 350 kV/m peak-to-peak were measured. The field sensing–detection process shows a good linearity in the range of 10–350 kV/m, as shown in Fig. 6. To illustrate the operation of the experimental setup, electric fields of 200 kV/m and different frequencies were measured. Fig. 7(a) and (b) illustrates the input and output waveforms for 100 Hz and 20 kHz, respectively. As can be observed in Fig. 7, the recuperated signal level is at 200 mV, and the ratio between the applied electric field and the recuperated signal is 10^6 (1/m) [120 dB (1/m)]. The noise level is about 2 mV. The SNR of the recuperated signal at 200 kV/m was better than 30 dB, being just proportional to the optical detected power. Using the linear response shown in Fig. 6, these data become a calibration factor for the proposed sensing system.

The minimum detected electric field was determined experimentally, and Fig. 8 depicts such a measurement for two crystal lengths; Fig. 8(a) shows the quasi-minimum detected signal for the 13-mm-long sensor when an 18-kV/m electric field is sensed. The sensitivity of the crystal sensor is related to its physical length, and in the aim of an objective comparison,

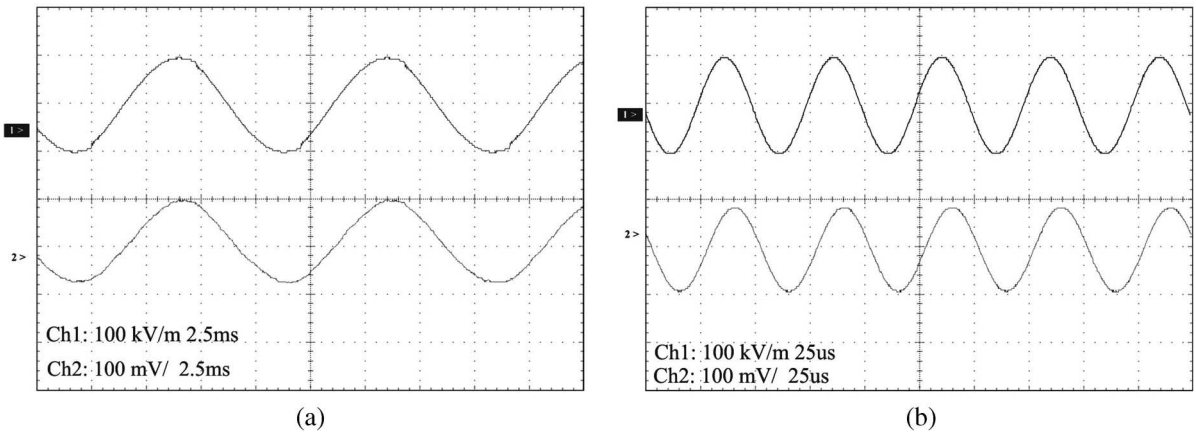

Fig. 7. Sensed and detected electric field waveforms (200 kV/m). (a) 100 Hz. (b) 20 kHz.

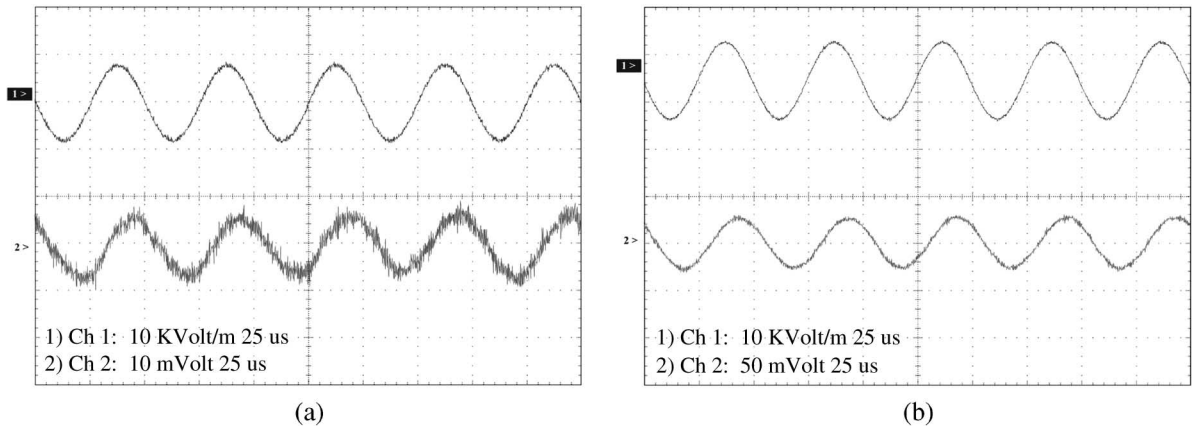

Fig. 8. Detected electric fields comparison, depending on the length of the sensors. (a) For 13 mm. (b) For 35 mm.

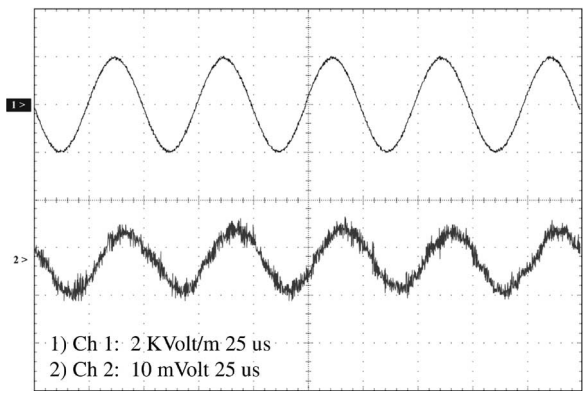

Fig. 9. Minimum electric field detection using a 35-mm-long sensor.

the 18-kV/m electric field was also sensed by a 35-mm-long sensor. Fig. 8(b) shows the recuperated signal in this case. For the same sensed electric field, the sensitivity of the shorter sensor is significantly lower than that for the longer one; this is concluded by comparing the recuperated amplitudes in both cases (14 mVpp and 60 mVpp, respectively), thus corresponding to a ratio of about 13 dB. As the longer crystal is more sensitive, its quasi-minimum detected electric field was also measured, being around 4 kV/m, giving a recuperated signal amplitude of 14 mVpp, as depicted in Fig. 9. This last measurement shows that sensitivity can be greatly improved by using the longest crystals that are available. The experimental minimum detected electric fields are higher than the values given in (8). The difference can neither be related to shot-noise-limited photodetection nor be due to an optimum sensing and optical modulation–demodulation process.

In our experimental setup, it is very well known that fiber polarizers and the electrooptic birefringent electrooptic retarders are sensitive to environmental variations. In particular, these elements are sensitive to temperature changes, which affect their performances. A potential long-term drift can be observed on the sensor and demodulator operating points. In our experiments, no severe drift has been observed, even if the system has been operating for several hours a day. However, to overcome the potential temperature dependence on the electrooptic crystals, polarization-independent electrooptic devices are being studied. Such devices are much less polarization sensitive and can be promising for the implementation of electric-field-sensing schemes of higher performance, using coherence modulation. Work in such a direction is in progress, and unbalanced Mach–Zehnder interferometers, using x-cut z-propagating $LiNbO_3$ modulators, are being tested in our laboratory.

V. Conclusion

A fiber and integrated optics coherence-modulated optical scheme for sensing high-intensity wideband electric fields has been reported here. The detection of high intensities and frequencies, ranging from 10 to 350 kV/m peak-to-peak and from 0 to 20 kHz, respectively, using coherence modulation of light and matched electrooptic retarders, has been successfully tested in our laboratory. Work is in progress to achieve larger bandwidths, e.g., in the megahertz range. In these kinds of sensing schemes, the bandwidth is only limited by the light transit time on the electrooptic sensor. $LiNbO_3$ electrooptic devices are inherently very wideband, responding potentially from dc to several gigahertz. The relative high-intensity operating range of our experimental scheme is determined by the use of short electrooptic crystals as the half-wave electric field is high. As demonstrated in the experimental results, longer crystals allow lower half-wave fields and, hence, the measurement of lower intensity electric fields.

This paper has presented potential applications of wideband coherence-modulated sensors in more complex schemes involving optical multiplexing to give distributed arrays of sensors, based on matched electrooptic sensors and demodulators, in fiber optic architectures. A fiber serial coherence multiplexing, in a simple array implementation, could be useful for detecting and analyzing multipoint electric fields in the electric power industry, in high-intensity electric field environments, for high-intensity telecommunication signals, etc. Work is also in progress to show multichannel all-fiber multiplexed sensing using almost all fiber optical components.

Acknowledgment

The authors would like to thank A. García-Juarez and L. A. Carcaño-Rivera (Ph.D. students at INAOE) for their support in pigtailing the electrooptic devices used in this paper.

References

[1] A. R. Johnston, H. Kirkham, and B. T. Eng, "DC electric field meter with fiber-optic readout," *Rev. Sci. Instrum.*, vol. 57, no. 11, pp. 2746–2753, Nov. 1986.

[2] H. Kirkham, "Measuring electric fields from power lines: Part I," *IEEE Instrum. Meas. Mag.*, vol. 9, no. 3, pp. 54–56, Jun. 2006.

[3] H. Kirkham, "Measurement of electric fields generated from alternating current," *IEEE Instrum. Meas. Mag.*, vol. 9, no. 5, pp. 58–61, Oct. 2006.

[4] H. Kirkham, "Dust devils and dust fountains: The measurement challenges," *IEEE Instrum. Meas. Mag.*, vol. 9, no. 6, pp. 48–52, Dec. 2006.

[5] C. J. Harland, T. D. Clark, and R. J. Prance, "Remote detection of human electroencephalograms using ultrahigh input impedance electric potential sensors," *Appl. Phys. Lett.*, vol. 81, no. 17, pp. 3284–3286, Oct. 21, 2002.

[6] T. Meier, C. Kostrzewa, K. Petermann, and B. Schuppert, "Integrated optical E-field probes with segmented modulator electrodes," *J. Lightw. Technol.*, vol. 12, no. 8, pp. 1497–1503, Aug. 1994.

[7] Y. J. Rao, H. Gnewuch, C. N. Pannell, and D. A. Jackson, "Electro-optic electric field sensor based on periodically poled $LiNbO_3$," *Electron. Lett.*, vol. 35, no. 7, pp. 596–597, Apr. 1, 1999.

[8] Y.-S. Yim, S.-Y. Shin, W.-T. Shay, and C.-T. Lee, "Lithium niobate integrated-optic voltage sensor with variable sensing ranges," *Opt. Commun.*, vol. 152, no. 4–6, pp. 225–228, Jul. 1, 1998.

[9] T.-H. Lee, F.-T. Hwang, W.-T. Shay, and C.-T. Lee, "Electromagnetic field sensor using Mach–Zehnder waveguide modulator," *Microw. Opt. Technol. Lett.*, vol. 48, no. 9, pp. 1897–1899, Sep. 9, 2006.

[10] K. Hidaka and H. Fujita, "A new method of electric field measurements in corona discharge using Pockels device," *J. Appl. Phys.*, vol. 53, no. 9, pp. 5999–6003, Sep. 1982.

[11] D. H. Naghski, J. T. Boyd, H. E. Jackson, S. Sriram, S. A. Kingsley, and J. Latess, "An integrated photonic Mach–Zehnder interferometer with no-electrodes for sensing electric fields," *J. Lightw. Technol.*, vol. 12, no. 6, pp. 1092–1098, Jun. 1994.

[12] F. Cecelja, M. Bordovsky, and W. Balachandran, "Lithium niobate sensor for measurement of DC electric fields," *IEEE Trans. Instrum. Meas.*, vol. 50, no. 2, pp. 465–469, Apr. 2001.

[13] J. Rodríguez-Asomoza and C. Gutiérrez-Martínez, "Electric field sensing system using a Ti:$LiNbO_3$ optical coherence modulator," in *Proc. IEEE IMTC*, Budapest, Hungary, May 2001, pp. 1075–1078.

[14] C. Gutiérrez-Martínez, G. Trinidad-Garcia, and J. Rodríguez-Asomoza, "Electric field sensing system using coherence modulation of light," *IEEE Trans. Instrum. Meas.*, vol. 51, no. 5, pp. 985–989, Oct. 2002.

[15] C. Gutiérrez-Martínez and J. Santos-Aguilar, "Wide-band electric fields sensing using coherence modulation of light," in *Proc. IEEE IMTC*, Como, Italy, May 2004, pp. 1882–1885.

[16] C. Gutiérrez-Martínez, H. Porte, and J. P. Goedgebuer, "A microwave coherence-multiplexed optical transmission system on Ti:$LiNbO_3$ integrated optics technology," *Microw. Opt. Technol. Lett.*, vol. 14, no. 1, pp. 64–69, Jan. 1997.

[17] I. P. Kaminow and J. Liu, "Propagation characteristics of partially loaded two-conductor transmission line for broadband light modulators," *Proc. IEEE*, vol. 51, no. 1, pp. 132–136, Jan. 1963.

[18] W. W. Rigrod and I. P. Kaminow, "Wide-band microwave light modulation," *Proc. IEEE*, vol. 51, no. 1, pp. 137–140, Jan. 1963.

[19] F. R. Nash and P. W. Smith, "Broadband optical coupling modulation," *IEEE J. Quantum Electron.*, vol. QE-4, no. 1, pp. 26–34, Jan. 1968.

[20] F.-S. Chen, "Modulators for optical communications," *Proc. IEEE*, vol. 58, no. 10, pp. 1440–1457, Oct. 1970.

[21] R. C. Alferness, "Waveguide electrooptic modulators," *IEEE Trans. Microw. Theory Tech.*, vol. MTT-30, no. 8, pp. 1121–1137, Aug. 1982.

[22] *Fiber Optic Test and Measurement*, D. Derickson, Ed. Upper Saddle River, NJ: Prentice-Hall PTR, 1998, pp. 246–283. Hewlett-Packard professional books.

[23] H. B. Killen, *Fiber Optics Communications*. Englewood Cliffs, NJ: Prentice-Hall PTR, 1991, pp. 43–68.

[24] I. Andonovic and D. Uttamchandani, *Principles of Modern Optical Systems*. Norwood, MA: Artech House, 1989, pp. 109–120.

[25] D. M. Baney, W. V. Sorin, and S. A. Newton, "High-frequency photodiode characterization using a filtered intensity noise technique," *IEEE Photon. Technol. Lett.*, vol. 6, no. 10, pp. 1258–1260, Oct. 1994.

[26] D. M. Baney and W. V. Sorin, "Broadband frequency characterization of optical receivers using intensity noise," *Hewlett-Packard J.*, vol. 46, no. 1, pp. 6–12, Feb. 1995.

[27] G. E. Obarski and P. D. Hale, "How to measure relative intensity noise in lasers," *Laser Focus World*, vol. 35, no. 5, pp. 273–277, May 1999.

Celso Gutiérrez-Martínez (M'88) was born in Oaxaca, México. He received the B.S. degree in electronics and communications engineering from the Instituto Politecnico Nacional (IPN), México City, México, in 1985, the M.S. degree in electrical engineering from Centro de Investigación y de Estudios Avanzados del Instituto Politecnico Nacional (CINVESTAV-IPN), Mexico City, in 1985, and the Ph.D. degree in "sciences pour l'ingenieur" from the Université de Franche-Comté, Besançon, France, in 1994.

Since November 1994, he has been with the Instituto Nacional de Astrofisica, Optica y Electronica (INAOE), Puebla, México, working in the fields of electronics, optics, and microwaves for telecommunications and signal processing.

Joel Santos-Aguilar was born in Puebla, México. He received the B.S. degree in electronics from the University of Puebla and the M.S. degree in electronics in 2005 from the Instituto Nacional de Astrofisica, Optica y Electrónica (INAOE), Puebla, where he is currently working toward the Ph.D. degree, working in optoelectronics and integrated optics for electric field sensing and radio-over-fiber systems.